ACS APPLIED MATERIALS & INTERFACES

Research Article

Cite This: ACS Appl. Mater. Interfaces 2019, 11, 3407−3416

www.acsami.org

Responsive Nanoporous Membranes with Size Selectivity and Charge Rejection from Self-Assembly of Polyelectrolyte "Hairy" Nanoparticles

Yulia Eygeris,[‡,†] Emily V. White,[‡,†] Qiaoyi Wang,[‡] John E. Carpenter,[‡] Michael Grünwald,*[,‡] and Ilya Zharov*[,‡,§,∥]

[‡]Department of Chemistry and [§]Department of Materials Science & Engineering, University of Utah, 315 South 1400 East, Salt Lake, Utah 84112, United States

[∥]A. M. Butlerov Chemistry Institute, Kazan Federal University, 18 Kremlyovskaya Street, Kazan 420008, Russia

Supporting Information

ABSTRACT: We report the preparation and characterization of charged nanoporous membranes by self-assembly of "hairy" silica nanoparticles (HNPs) functionalized with polyelectrolyte copolymer brushes. We show that HNP membranes possess high water flux, have well-defined pore sizes, and rejection up to 80% of charged species in solution. The properties of these membranes can be tuned by controlling the length and composition of polymer brushes and the electrolyte concentration in solution. We demonstrate that membrane pore sizes undergo changes of up to 40% in response to changes in the ionic strength of the salt solution. Using MD computer simulations of a coarse-grained model, we link these tunable properties to the conformations of polymer chains in the spaces between randomly packed HNPs. As polymer length increases, the polymers fill the interparticle gaps, and the pore size decreases markedly. On the basis of their straightforward fabrication and tunable properties, HNP membranes may find applications in size- and charge-selective separations, water desalination, and responsive devices.

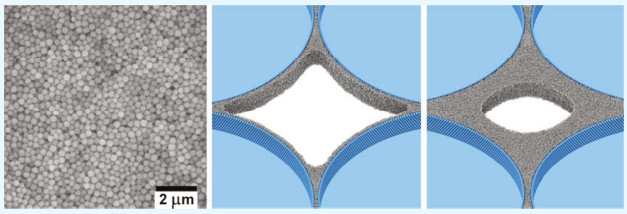

KEYWORDS: *nanopore, membrane, nanoparticle, polyelectrolyte, permeability, polymer brush*

INTRODUCTION

Nanoporous membranes provide significant economic, operational, and environmental advantages in separations because their application is relatively simple and allows saving energy, space, and materials.[1] Membrane separations rely on size and charge exclusion and require large permeability and rejection of target solutes,[1,2] which in the case of nanoporous membranes include suspended solids, bacteria, viruses, and ions.[3] Because of their separation ability, nanoporous membranes find applications on the industrial and laboratory scale in water and wastewater treatments, food engineering,[1] biotechnology,[4] biosensing,[5] drug delivery,[6] and catalysis.[7] All these applications require precise control over the pore size in a wide range, a narrow pore size distribution and functional pore surfaces,[6] and would greatly benefit from a simple and economical preparation of the membranes.

Most commercial nanoporous membranes are created from polymeric materials using phase inversion and casting processes.[8,9] These processes are quite complicated and do not allow precise control of the membrane's pore size and surface chemistry.[9,10] Thus, new approaches to the preparation of nanoporous membrane materials attract growing attention.[11,12] In particular, self-assembly promises many advantages for nanoporous membrane preparation in terms of fabrication, processing, cleaning, and reuse of the membranes. As a versatile preparation method, self-assembly has been used to fabricate nanoporous membranes from small molecules,[13] liquid crystals,[14] proteins,[15] dendrimers,[16] block copolymers,[17] anionic polymers,[18,19] and polyelectrolytes via layer-by-layer deposition.[20]

However, pore sizes of membranes prepared by self-assembly of molecular building blocks are firmly set by the size of the molecules; controlling the membrane pore size thus usually involves a change of molecular building blocks and associated cumbersome changes in the synthetic protocol. Assembling nanoporous membranes from nanoscale building blocks, such as surface-functionalized nanoparticles, provides an attractive alternative.[21,22] These building blocks cover a wide range of sizes and compositions and thus enable a straightforward preparation of membranes with a wide range of nanopore sizes and diverse surface chemistry.[23]

The main challenge in the preparation of membranes from nanoparticles is mechanical stability. When layered as a film, nanoparticles only interact weakly through van der Waals interactions and thus do not provide stable membranes. This problem can be addressed by chemical cross-linking, as

Received: October 7, 2018
Accepted: December 27, 2018
Published: December 27, 2018

DOI: 10.1021/acsami.8b17483
ACS Appl. Mater. Interfaces 2019, 11, 3407−3416

demonstrated for carboxylated silver nanoparticles using amide bond formation[24] and for silica nanoparticles (SNPs) using high-temperature sintering.[25,26] An alternative solution is to increase the strength of non-covalent interactions between nanoparticles. This can be achieved using layer-by-layer self-assembly of nanoparticles,[27,28] which was shown to lead to membranes with enhanced separation performance, reduced fouling, antimicrobial activity, and novel functionality.[3]

Our strategy is to use polymer brushes attached to the nanoparticle surface as a "molecular glue" to increase the mechanical stability of nanoparticle assemblies. This strategy exploits non-covalent polymer−polymer interactions, which depends on the composition, length, and grafting density of polymer brushes, as well as on the solvent.[29−32] In earlier work, we demonstrated that SNPs grafted with short polymer brushes form robust nanoporous membranes via reversible nanoparticle assembly in both organic solvents and water, exploiting electrostatic and hydrophobic interactions, respectively.[33] However, the role of those short polymer brushes was limited to increasing the mechanical stability of the assemblies, and they did not affect the nanopore size or functionality.

Introducing charges to the nanopore surface creates membranes that act as ion channel analogs capable of selective ion transport. Such synthetic ion channels have been prepared in a variety of geometries and materials, including cylindrical nanotubes,[34] conical inorganic nanopores,[35] and also colloidal nanopores.[36] The latter was prepared by decorating the surface of silica colloidal crystals with charged moieties, such as amines[37,38] and sulfonic groups.[26] These membranes impede the transport of like-charge species and enhance ionic transport selectivity through their tortuosity. The same principles have been applied in polymeric nanoporous membranes with charged surfaces, resulting in improved charge rejection and reduced fouling.[6]

To prepare polymer brush nanoparticle membranes with charged nanopores, polymer brushes need to carry charged functional groups. For the present study, we selected polysulfonic acids because of the low pK_a of sulfonic groups, which assures their negative charge in water. Furthermore, it is known that polysulfonic acids change their conformation in response to the ionic strength of the solution.[39,40] We hypothesized that such conformational changes would affect the pore size in the membrane, leading to tunable size rejection.

Although polyelectrolyte brushes should provide high charge density on the nanopore surface, they may decrease the mechanical stability of the membrane, which is based on the cohesive forces between polymers. Polyelectrolytes are highly hydrophilic,[40] which may lead to "hairy" silica nanoparticles (HNPs) that are effectively repulsive in water and cannot be assembled into stable membranes. Therefore, a second hydrophobic monomer has to be used as part of the polymer brushes, to offset the charged species' hydrophilicity and to prevent membrane disassembly in water, similar to that described previously for HNP membranes stable in water and prepared using poly(2-hydroxyethyl methacrylate) brushes.[33] The mole ratio of the two monomers can be optimized to achieve the desired membrane properties.

In the following, we describe the preparation and properties of charged nanoporous membranes created from HNPs functionalized with polyelectrolyte copolymer brushes. We demonstrate that these membranes allow for large flux and enable large degrees of charge rejection. We present evidence that the membranes have pore sizes and charge rejection behavior that can be manipulated by tuning the polymer length and ionic strength of the solution. These properties are tightly linked to conformations of polymers in the voids between nanoparticles.

MATERIALS AND METHODS

Materials. 3-Aminopropyltriethoxysilane (APTES), triethylamine, 2-bromoisobutyryl bromide, 3-sulfopropyl methacrylate potassium salt (SPM), 2,2′-bipyridine, 2-ethoxyethyl methacrylate (EEMA), copper(I) chloride, and monodisperse dextrans of various molecular weights were purchased from Sigma Aldrich. 4-Dimethylaminopyridine (DMAP) and tetraethoxysilane were purchased from Alfa Aesar. Dichloromethane (DCM), methanol, ammonium hydroxide solution, tetrahydrofuran, sodium chloride, sodium sulfate decahydrate, and sodium citrate dihydrate were purchased from Fisher Chemicals. Copper(II) chloride dihydrate was purchased from Acros. Gold nanoparticles were purchased from BBI Solutions, and polystyrene spheres were purchased from Polysciences, Inc.

Characterization. SEM (Hitachi S3000-N) was used to image the HNP membranes. TGA of polymer-modified particles was conducted using a TGA 2950 Thermogravimetric Analyzer from TA Instruments. A Branson 1510 sonicator was used for all sonications. UV−vis measurements were performed using an Ocean Optics USB4000 instrument.

Preparation of Silica Particles. SNPs were prepared using the Stöber method.[41] The size of nanoparticles was determined by DLS and confirmed by TEM using a JEOL JEM-1400 instrument.

Grafting of Polymerization Initiator Moieties. Atom-transfer radical polymerization (ATRP) sites were prepared through previously described procedures in two steps.[33] In the first step, primary amines were grafted on the surface to facilitate the addition of initiator sites as follows: A suspension of ∼2 g of Stöber silica particles in 15 mL of dry acetonitrile was purged with nitrogen gas for 15 min, and then 0.2 mL of APTES was injected into the mixture. The reaction mixture was stirred for 24 h. Aminated particles were collected by centrifugation, washed at least three times with acetonitrile, and dried.

In the second step, polymerization initiator sites were grafted to the surface of the silica particles as follows: to a suspension of ∼1 g of aminated silica particles in 50 mL of anhydrous DCM, 40 mg (0.3 mmol) of DMAP was added, the reaction mixture was purged with nitrogen gas for 15 min, and 2.09 mL (15 mmol) of triethylamine and 1.61 mL (13 mmol) of 2-bromoisobutyryl bromide were injected. The reaction mixture was left to stir at room temperature for 24 h. The resulting particles were collected by centrifugation, washed at least three times with DCM, and then dried. Successful surface modification during each step was confirmed using TGA.

Polymerization. Polymer brushes were grafted through surface-initiated ATRP (SI-ATRP).[42] In a typical copolymerization run, 1 g of silica with initiator sites was combined with 16 mg (0.1 mmol) of $CuCl_2{\cdot}2H_2O$, 250 mg (1.6 mmol) of 2,2′-bipyridine, and 20 mmol of a monomer mixture (SPM and EEMA) in 12 mL of (2:1) MeOH−H_2O mixture. The desired degree of sulfonation was achieved by controlling the ratio of introduced monomers as their polymerization rates are similar.[43] Then, the reaction mixture was degassed by two freeze−pump−thaw cycles, and 27 mg (0.3 mmol) of CuCl was added to the mixture. The reaction mixture was left to stir at room temperature under nitrogen. Hairy particles were collected by centrifugation, washed twice with MeOH and H_2O, and left to stir overnight in 1 M HCl. Collected particles were washed twice with H_2O, once with MeOH, and then dried. The degree of polymerization was calculated using TGA, assuming a polymer grafting density of 0.2 nm^{-2}.[40]

Membrane Preparation. Dead-end filtration cells (10 mL; Sterlitech Corporation and Millipore Amicon) were used to prepare and study the HNP membranes. A membrane layer was prepared through pressure-driven deposition of a suspension of 30 mg of nanoparticles in 10 mL of 20% EtOH/H_2O onto a nylon support with

DOI: 10.1021/acsami.8b17483
ACS Appl. Mater. Interfaces 2019, 11, 3407−3416

a nominal pore size of 0.22 μm (Tisch Scientific, North Bend, OH; pore size determined using the bubble point method). The applied pressure was set to 1 bar. During the permeability experiments described below, the filtration cells were not stirred and we did not observe any significant nanoparticle loss (measured by mass). Final membranes were prepared by consecutive deposition of bare silica particles and HNPs, as described in the main text.

Membrane Testing. Water with a nominal resistivity of 18 MΩ·cm was used in the preparation of all solutions and water flow experiments. The applied pressure was set to 1 bar. Water flow was measured by driving pure water through the membrane and weighing collected fractions over time. Aqueous solutions of NaCl, Na_2SO_4, and $Na_3C_6H_5O_7$ were used to evaluate charge rejection. Five milliliters of each solution was driven through the membrane, and the permeate salt concentration was monitored over time using a conductivity meter (HM Digital, Inc., Culver City, CA). The rejection was determined as follows

$$R = \left(1 - \frac{C_p}{C_f}\right) \times 100\% \quad (1)$$

where C_p and C_f are the concentrations in permeate and feed, respectively. The salt concentration is linearly related to conductivity in this concentration range.

The pore size cutoff was determined using 0.5 g/L solutions of dextrans with different molecular weights (25, 80, 270, and 670 kDa) and a polystyrene sphere suspension in water (0.2% by weight). Five milliliters of solution was driven through the membrane under 1 atm applied pressure, and the amount of permeate was determined spectrophotometrically, at a wavelength of 492 nm for dextrans using the phenol–sulfuric acid method[44] and at a wavelength of 240 nm for polystyrene spheres. The reported values for dextran and salt rejection refer to the first milliliter of permeate, as rejection declines over time because of concentration polarization across a membrane. Rejection is calculated using the general formula described above.

Modeling. Polymers are modeled as linear chains of beads interacting via a cut and shifted Lennard–Jones potential with parameters ε = 1.5 kJ mol^{-1}, σ = 0.816 nm, and cutoff r_{cut} = 2.304 nm. Adjacent beads along polymer chains are linked by a harmonic potential $U_{bond} = \frac{1}{2}k(r - r_0)^2$, with k = 14600 kJ mol^{-1} nm^{-2} and r_0 = 0.5414 nm. Bond angles were enforced via a harmonic potential $U_{angle} = \frac{1}{2}k[\cos(\varphi) - \cos(\varphi_0)]^2$, with k = 25 kJ mol^{-1} and φ_0 = 131°. This model coarse-grains the polymers used in our experiments at a resolution of 1.92 monomers per model bead, that is, a polymer of 100 monomers corresponds to a chain of 52 coarse-grained beads in our model.

We parametrized this model in the following way. A recently reported MARTINI model[45] for PMMA was used as the starting point. To construct a model for the copolymer used in our experiments from this PMMA model, two additional MARTINI beads (types Q and Na)[46] were added to the PMMA backbone, representing the sulfopropyl and ethoxyethyl groups. These beads were distributed randomly across the polymer backbone to produce a ratio of 17% SPM/EEMA. Using this coarse-grained MARTINI model, we created a system of 200 polymers of 100 monomers each and measured the bulk density of the polymer in long NPT MD simulations in ambient conditions using the simulation package HOOMD.[47,48] These calculations yielded an amorphous solid with a density of 0.83 g cm^{-3}.

In a second coarse-graining step, we reduced the resolution of the MARTINI model further, aiming to preserve its bulk density. Starting from a linear chain of backbone beads taken from the PMMA model, we proportionally increased the bond length and non-bonded Lennard–Jones interaction parameter σ of backbone beads and reduced the number of beads along the polymer accordingly to keep the total stretched polymer length fixed. The final coarse-grained model (with a resolution of 1.92 monomers per model bead) matches the density of the MARTINI model in the solid state. To model the effects of solvation, the MARTINI non-bonded Lennard–Jones parameter ε was reduced to a value of 1.5 kJ mol^{-1}. This value results in polymer brush conformations that are an intermediate between the stretched state typical for highly charged polyelectrolyte brushes[49] and the collapsed brush characteristic of a non-polar polymer in water.

To reduce computational cost due to large system sizes, we do not model the entire spherical nanoparticles but focus our attention on the plane of contact of four nanoparticles. Specifically, we model a spherical nanoparticle as a periodically replicated cylinder with 270 nm diameter and 20.78 nm height. 3500 "anchor" beads were placed on the surface of nanoparticle cylinders in a close-packed arrangement. To each of these beads, a single polymer was attached via a harmonic spring (k = 14600 kJ mol^{-1} nm^{-2}; r_0 = 1.47 nm), resulting in a grafting density of 0.2 nm^{-2} and a total number of particles of up to ~900000 beads, depending on the polymer length. Non-bonded anchor and polymer beads interacted via a Lennard–Jones potential with ε = 2.7 kJ mol^{-1} and σ = 1.6 nm. We initialized all simulations by placing a single nanoparticle cylinder in a periodically replicated rectangular box with dimensions L_x = 400 nm, L_y = 400 nm, and L_z = 20.78 nm. Nanoparticles were treated as rigid bodies and were held fixed throughout the simulation. Polymers were first equilibrated at constant volume and a temperature of 300 K for 0.5 ns. After equilibration, the system was further equilibrated under NPT conditions (keeping L_z fixed) at 300 K and 1 atm pressure. During these simulations, which were run up to 100 ns, the simulation box would shrink and the nanoparticle would form a pore with its own periodic images. All simulations were performed with a time step of 5 fs using NVT/NPT integrators implemented in HOOMD-blue[47,48] on NVIDIA Tesla V100 GPUs at the Center for High-Performance Computing at the University of Utah.

RESULTS AND DISCUSSION

Preparation and Properties of Charged HNPs

Preparation of charged HNPs was accomplished as shown in Scheme 1. SNPs were prepared using the Stöber method[41] and had diameters of 267 ± 25 nm as confirmed by DLS and TEM. Silica particles were functionalized with amine groups followed by polymerization initiator moieties, as reported earlier.[33] Next, we carried out the SI-ATRP on the initiator-modified particles. We have selected two monomers: SPM, the source of negatively charged groups in the polymer brush, and EEMA, introduced to adjust the hydrophilicity of the polymer. The monomer ratio in this copolymer was set by adjusting the ratio of the monomers because their polymerization rates are similar, as we reported earlier.[43] We were able to control the

Scheme 1. Preparation of PSMP-*co*-PEEMA HNPs

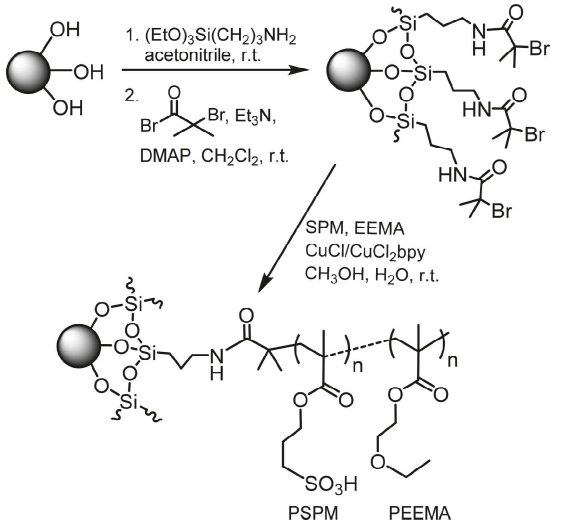

DOI: 10.1021/acsami.8b17483
ACS Appl. Mater. Interfaces 2019, 11, 3407–3416

degree of polymerization using the reaction time because of the controlled "living" nature of the polymerization. The degree of polymerization was established using TGA, assuming a grafting density of 0.2 polymer chains/nm^2 as was reported previously.[40]

We will refer to the resulting particles and the corresponding membranes by the average degree of polymerization and the percent of SPM monomers in the copolymer brush. For instance, HNPs made from polymers composed of 100 monomers at 17% SPM content will be labeled 100-17%.

To characterize the charge distribution in HNPs, we measured their ζ-potentials in aqueous solutions of NaCl of different concentrations (Figure 1). As expected, all tested

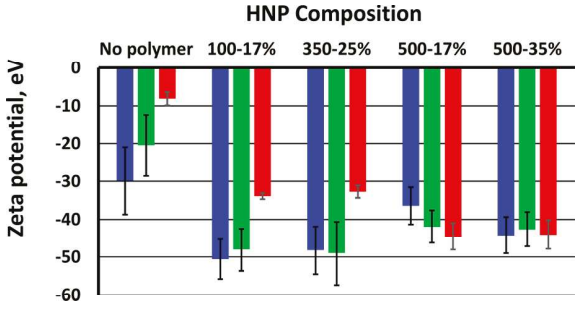

Figure 1. ζ-potential values of HNPs as a function of NaCl concentration (blue: 1 mM; green: 10 mM; red: 50 mM).

samples showed negative ζ-potentials because of the presence of hydroxyl groups on the surface of silica particles and sulfonic acid groups of the polymer. However, samples responded differently to changes in the electrolyte concentration. Bare silica particles and particles with 100-17% and 350-25% brushes showed decreasing ζ-potentials with increasing electrolyte concentration, likely because of charge screening. However, HNPs containing the longest brushes (500-17% and 500-35%) did not show any significant response to the change in salt concentration. We speculate that this unusual behavior is a result of polymer conformation response to the presence of the electrolyte.

Using the measured ζ-potential, we have calculated the net charge density σ for each sample via $\sigma = \xi\varepsilon_w/\lambda_D$, where ξ is the ζ-potential, ε_w is the dielectric constant of water, and λ_D is the Debye length. Results are presented in Figure 2. The presence of the polymer increases the net charge density up to five times compared to the bare silica spheres, and charge density

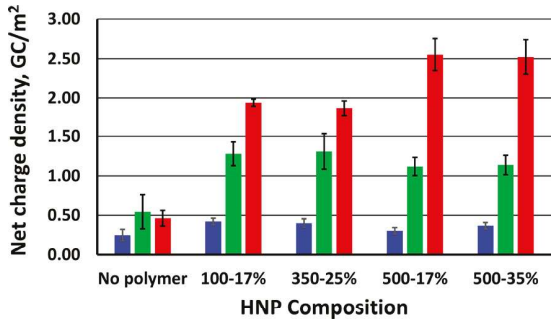

Figure 2. Net charge density of HNPs calculated from their ζ-potentials for different NaCl concentrations (blue: 1 mM; green: 10 mM; red: 50 mM).

increases for all HNP samples with increasing salt concentration. However, neither the polymer length nor the degree of sulfonation was found to have a strong influence on charge density, likely because of the charge screening. The net charge density of HNPs, as measured via ζ-potential, describes the electric properties of free particles in solution and cannot be directly converted to a surface charge density of densely packed HNP membranes. However, the charge density of HNPs predicts a substantial negative surface charge for HNP membranes and a potential dependence of membrane behavior on polymer brush length.

HNP Membrane Formation. Hairy particle membranes can be easily assembled by pressure-driven deposition of HNP solutions onto macroporous supports like nylon.[33] We found that, to obtain HNP membranes that reproducibly adhere to the nylon support, an underlayer of bare SNPs is beneficial. In all our experiments, we thus prepare membranes by consecutive deposition of a support layer of bare SNPs of approximately 70 μm thickness, followed by HNPs, resulting in a final membrane of approximately 150 μm thickness.

The SPM content of polymer brushes directly affects the solubility of HNPs and thus should have a marked influence on the morphology of self-assembled structures. Top-view SEM images of different self-assembled HNP arrays indeed confirm this notion, as illustrated in Figure 3, and side-view SEM images are shown in Figure S1 (see the Supporting Information). Assemblies containing the shortest polymer brushes with the smallest degree of sulfonation (50-10%) showed highly irregular particle packing characteristic of strongly attractive interactions between HNPs. (HNPs with zero SPM content are not stable in water.) By contrast, HNPs with brushes of the same polymer length but a higher degree of sulfonation (50-17%) provided more regular particle packings with short-range close-packed crystalline order. We attribute this effect to increased electrostatic repulsion between HNPs that offsets attractive forces between hydrophobic EEMA monomers. Increasing the polymer length and degree of sulfonation produced structures of similar short-range order. A further increase in SPM content did not improve the degree of order in HNP assemblies; in particular, we did not observe well-developed colloidal crystals for any of the HNPs we tested. Side-view SEM images (Figure S1) show closed-packed particles but no ordering similar to that described above, which appears to be due to the way the membranes break onto the uneven surfaces. Side-view images also show that there was no separation between the SNP and HNP layers of the membranes. For our membrane permeability studies, we settled on membranes assembled from HNPs with the degree of polymerization between 100 and 500 monomers and SPM content between 17 and 35%.

The formation of randomly packed colloidal crystals can be attributed to the polymer length and conformation.[50] Depending on the degree of polymerization, particle size, and grafting density, polymer brushes can take either stretched (concentrated) or relaxed (semidilute) conformation. The Daoud–Cotton scaling model describes the critical polymer length below which the polymer is stretched.[51,52] According to the scaling model, the prepared sulfonated brushes are in a relaxed conformation, which would enable free movement of polymer chains and a lesser degree of order in colloidal crystals,[52] which is in agreement with the disordered packing observed by SEM. Although this is potentially detrimental to the mechanical stability of the hairy particle membranes, we found that, even

DOI: 10.1021/acsami.8b17483
ACS Appl. Mater. Interfaces 2019, 11, 3407–3416

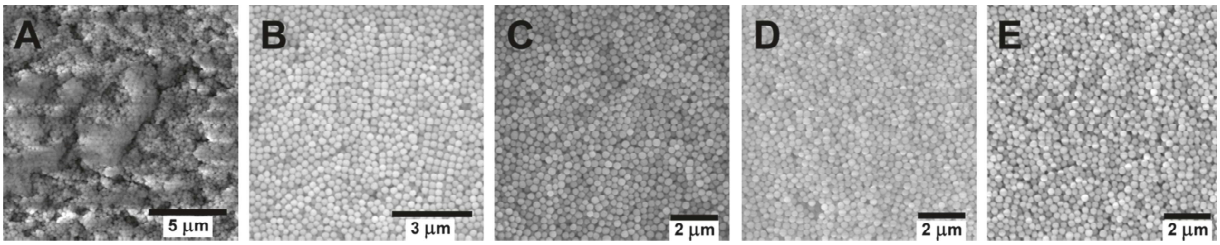

Figure 3. SEM images of particle arrays prepared with (A) 50-10% HNPs, (B) 50-17% HNPs, (C) 100-17% HNPs, (D) 350-25% HNPs, and (E) 500-35% HNPs.

Table 1. Flux and Permeability Results

membrane (DP-%SPM)	J, L m^{-2} h^{-1}	R_M, 10^{15} kg m^{-1} s^{-1}	R_S, 10^{15} kg m^{-1} s^{-1}	κ, nm^2
bare silica	226 ± 18	73 ± 6		39 ± 3
100-17%	103 ± 5	139 ± 11	67 ± 3	38 ± 2
350-25%	50 ± 2	287 ± 11	208 ± 8	18 ± 1
500-35%	11 ± 1	1303 ± 118	1236 ± 112	4 ± 1

with the very short polymer brushes (50 monomers per brush), these membranes can be handled, sandwiched, transferred, and even dropped without significant damage.[33]

One of the most important characteristics of a membrane is solute transport, which can be described in terms of steric and electrostatic rejection.[53] The steric model simply states that a solute with radius r_{solute} that is larger than the typical pore radius r_{pore} will be retained by the membrane. The electrostatic model takes into account the interactions between the solute and membrane surface charges.[54] Below, we describe the size exclusion and charge rejection characteristics of our HNP membranes.

Water Flux and Permeability of HNP Membranes. Water flux is an essential membrane performance parameter that also provides insight into the membrane structure and integrity. To characterize the influence of polymer brushes on membrane behavior, we measured the water flux J through the layer of bare silica spheres and through the membrane composed of HNPs and bare silica layers. The bare silica layers were prepared using particles of the same size as the HNP cores. Water flux through these layers was consistent but showed small variations (from 208 to 244 L m^{-2} h^{-1}) from sample to sample, likely because of minor variations in particle packing. The flux through the HNP membranes, however, changed dramatically depending on the polymer brush composition, ranging from 11 to 103 L m^{-2} h^{-1}. These flux values are comparable to those of commercially available ultrafiltration membranes (34 to 102 L m^{-2} h^{-1}).[55] Results of our flux measurements are summarized in Table 1.

Membrane resistance to the flow R can be calculated as $\Delta P/JAL$ for a membrane with thickness L under applied pressure ΔP (1 atm in our experiments). In our membranes where fluid passes through sequential layers of bare and hairy nanoparticles, the overall resistance is the sum of the contribution of individual layers is

$$R_M = R_B + R_S \tag{2}$$

where R_M is the membrane resistance, R_B is the resistance of the bare silica layer ($R_M = R_B$ for the bare silica membrane in Table 1), and R_S is the resistance of the hairy particle layer.

Clearly, polymer brushes affect the flow impedance. Although short 100-17% brushes do not have a statistically significant effect compared to bare silica, 350-25% and 500-35% increase the resistance ca. 3 and 17 times, respectively. The effect of polymer brush length is nonlinear in agreement with the polymer brush conformation theory prediction; for semidilute or relaxed polymer brushes, the polymer thickness h is $\sim N^{0.5}$, where N is the degree of polymerization.[52]

To account for the changes in membrane thickness and to assess the effect of different polymers on water flux, we calculated membrane permeabilities κ as described by Darcy's law

$$\kappa = J\mu L/\Delta P \tag{3}$$

where μ is the viscosity of water.

Decreasing permeabilities is directly linked to decreasing membrane pore sizes. We estimated pore sizes from permeability data using two mathematical models, the capillary tube (CT) model and the Kozeny–Carman (KC) model. The CT model describes membrane pores as capillary tubes of well-defined diameter (i.e., pore size) and tortuosity. Assuming Hagen–Poiseuille flow and using Darcy's law, the pore radius in the CT model can be described as

$$R_{pore}^2 = 8\kappa\tau/\varepsilon \tag{4}$$

where ε is the porosity of the system, τ is the tortuosity, and κ is the permeability described above. We estimate the porosity of a solid composed of randomly close-packed spheres coated with a polymer to be 0.30 and its tortuosity to be ~1.9.[56] On the basis of this model, HNP membranes with 500-35% and 100-17% brushes have pore diameters of ~28 and ~88 nm, respectively, as shown in Table 2.

The KC model is commonly used to describe fluid flow through a bed of packed particles. The advantage of this model

Table 2. Pore Sizes Estimated Using Different Models for $D_{particle}$ = 267 nm, ε = 0.30, τ = 1.9, κ_o = 38, and κ = 4 nm^2 for the HNP Membrane (500-35% Brush) and a Layer of Bare SNPs

	estimated pore diameter, nm	
method	HNPs	SNPs
CT model	~28	~90
KC model	~32	~101
size rejection	31–54	~100[58]

DOI: 10.1021/acsami.8b17483
ACS Appl. Mater. Interfaces 2019, 11, 3407–3416

is that particle shape and pore connectivity can be taken into account explicitly. For spheres, however, the relationship between the permeability and pore size reduces to a formula that is essentially identical to the CT model

$$R_{\text{pore}}^2 = 4\kappa K/\varepsilon \quad (5)$$

where K (= 4.8) is the Kozeny constant.[57] HNP membrane pore diameters calculated based on this model are ∼32 nm for 500-35% brushes and ∼99 nm for 100-17% brushes, in good agreement with the CT model.

Comparison of the pore size in the HNP membrane to that in a bare silica membrane further reveals the effect of the polymeric molecular glue in the membrane. Pore sizes for the bare SNP membrane were calculated on the basis of water flux using both the CT and KC model and are ∼90 and ∼101 nm, respectively, which are in good agreement with previous experimental results based on size rejection.[58] These values are similar to those obtained for short polymer brushes (100-17%). Long 500-35% polymers, on the other hand, have pores with much smaller diameters, strongly suggesting that polymer chains fill the interparticle spaces.

Filtration Cutoff of HNP Membranes. Pore size is an important characteristic of membranes used in size-based separations. Even though the pore size in HNP membranes can be estimated on the basis of water permeability as described above, it is important to establish the pore size more directly, because nanoscale systems may deviate in unexpected ways from model predictions and because pore geometry may affect solute retention.[59] One way to determine the pore size directly is by testing the rejection of solutes of known sizes, such as polystyrene beads, or solutes with known molecular weight, such as proteins or dextrans.[60]

First, we tested the permeation of dextrans through 500-35% HNP membranes. We monitored the permeation of dextrans with molecular weights between 25 and 670 kDa. We found no significant dextran retention (R_{ave} ∼18%), no correlation of retention with molecular weight, and no change in water flux throughout the experiments. The dextran radius can be estimated on the basis of its molecular weight according to

$$r_{\text{dex}} = 0.33 M_{\text{w}}^{0.46} \quad (6)$$

where r_{dex} is the radius of dextran molecules in Å and M_{w} is the molecular weight in g mol^{-1}.[61] Thus, the diameter of dextrans used in our experiments varied from 7 to 31 nm, suggesting that 500-35% HNP membranes contain nanopores larger than 31 nm.

To further characterize the pore size in 500-35% HNP membranes, we monitored the permeation of 54 nm polystyrene beads, which were completely retained by the membrane. Taken together, our rejection experiments show that the membrane pore size is between 31 and 54 nm, in good agreement with the pore size calculated based on water permeability of HNP membranes. The somewhat smaller pore size estimated using the CT and KC models may be because these models do not take into account slip flow inside the nanopores.[62]

Modeling of Nanopores in HNP Membranes. To reveal the polymer configurations that are responsible for the observed dependence of water flux and pore size on polymer length, we have performed MD computer simulations with a coarse-grained model of nanoparticles and polymers (see Materials and Methods). We focus on polymer configurations within a pore formed by nanoparticles arranged on a square lattice, as illustrated in Figure 4A. This particular geometry

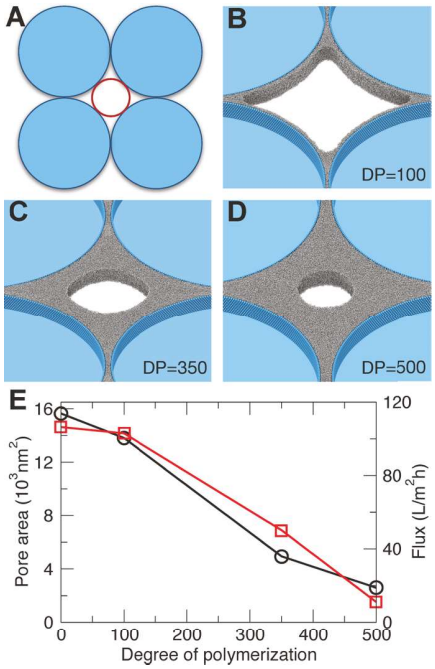

Figure 4. (A) Illustration of a pore formed by four nanoparticles (blue circles). The size of the largest sphere that will pass through the pore is indicated in red. (B–D) Snapshots from MD simulations of a pore formed by HNPs with different degrees of polymerization. Nanoparticles (blue) are modeled as rigid cylinders (see Materials and Methods); polymer chains are shown in gray. (E) Plot of the experimentally measured flux (red squares) and pore sizes measured in simulations (black circles), as a function of polymer length. The flux for DP = 0 was estimated by extrapolating data for bare silica layers to a membrane thickness of 150 μm.

serves as a simple model for more complicated pore geometries encountered in a random packing of spherical nanoparticles. For nanoparticles with 267 nm diameter, the largest sphere that can pass through such a pore has a diameter of 110 nm, consistent with the pore size based on rejection measurements for bare silica membranes (Table 2). Next, we analyzed how the geometry and size of the pore change in the presence of polymer. In Figure 4B–D, we show equilibrium configurations of our model polymers with degrees of polymerization identical to polymer brushes used in our experiments (100/350/500). Although the shortest polymers do not change the shape and size of the pore significantly, longer polymers partially fill the space between nanoparticles and result in pores that have a circular cross section, reflecting the tendency of the polymer to reduce the size of the interface with the surrounding solution. The longest polymer (500 monomers) results in a pore with 57 nm diameter, similar to but somewhat larger than our experimental estimate of 31–54 nm based on size exclusion. By assuming that the water flux through these pores is proportional to the cross-sectional area of the pore, we can nevertheless compare the dependence of pore size on polymer length with the experimental data; as illustrated in Figure 4E, the trends found in our experiments are well reproduced by the simulations. Note, however, that this analysis neglects water flux through the viscous polymer brush.

DOI: 10.1021/acsami.8b17483
ACS Appl. Mater. Interfaces 2019, 11, 3407–3416

Furthermore, flux through our HNP membranes is determined not only by the pore geometry considered here but also by a network of pores of different sizes and shapes, with different degrees of polymer filling. For instance, our simulations suggest that the smaller triangular voids formed by three close-packed HNPs are completely filled by polymers composed of 350 monomers or more.

Responsive Nanopore Behavior in HNP Membranes. Charged polymer brushes are known to undergo conformational changes in the presence of electrolytes. For example, positively charged brushes grafted onto a planar surface were observed to swell when salt concentration was increased and then suddenly collapsed at concentrations of tens of millimolars.[49] This behavior can be explained by a competition of charge screening and osmotic pressure. A similar observation has been made for negatively charged brushes.[39]

This peculiar behavior of polyelectrolyte brushes can have a significant effect on the size of the pores in HNP membranes and their separation properties. To test whether pSPM-*co*-pEEMA brushes experience conformational changes inside the HNP membranes in the presence of salt, we measured the flux of aqueous NaCl solutions of different concentrations through HNP membranes. We observed a decrease in water transport through the membranes: flux through 100-17% membranes decreased from 103 to 65 L m^{-2} h^{-1} and from 11 to 4 L m^{-2} h^{-1} for 500-35% membranes when NaCl concentration increased from 0 to 100 mM, as illustrated in Figure 5. This

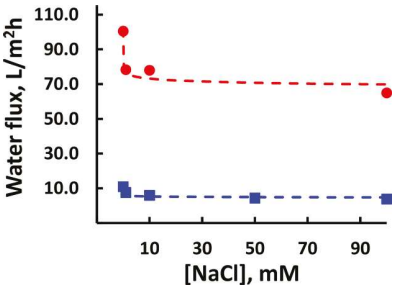

Figure 5. NaCl solution flux as a function of concentration for 100-17% (red circles) and 500-35% HNP membrane (blue squares); dashed lines are exponential fits used as a guide for the eye.

result indicates a partial pore blockage likely related to swelling of polymer brushes. Using the KC model, we estimate that the average pore diameter decreases by ca. 40 nm for 100-17% HNP membranes and by ca. 20 nm for 500-35% HNP membranes. The different response of short and long polymer brushes is analogous to the behavior reported for poly(3-sulfopropyl methacrylate) brushes on flat surfaces[63] and for poly(*N*-isopropylacrylamide) brushes inside the colloidal nanopores.[64] In the latter case, this difference was explained by the ability of short polymer brushes to freely change their conformation in response to temperature changes, while long polymer brushes filled the pores, which precluded conformational changes.

We note that we did not find evidence of polymer brush collapse at high salt concentrations, as reported for polymer brushes on flat surfaces.[39,65] However, these reports involved considerably longer polymer brushes and higher salt concentrations.

We further confirmed the notion of polymer brush swelling by measuring the rejection of dextrans in the presence of salt. For this experiment, we chose the largest dextran (670 kDa) that was observed to pass through the membrane in the absence of salt. A solution of dextran and sodium citrate (1:1 by volume stock solutions of dextran and 10 mM sodium citrate) was pushed through the membrane containing 500-35% brushes, as this membrane showed the largest response to the presence of salt solution. We observed a dextran rejection of 60% compared to 18% in pure water. This significant change is a clear indication of reduced pore size.

Charge Rejection in HNP Membranes. Membranes containing charged nanopores are in principle capable of salt rejection by hindering the transport of co-ions due to electrostatic repulsion.[66] Utilizing this separation mechanism in ultrafiltration membranes could offer advantages over reverse osmosis membranes because it would require much lower operating pressures to maintain high flux.[67] To evaluate the ability of charged HNP membranes to reject salts, we measured the permeation of three strong electrolytes (sodium chloride, sulfate, and citrate) at different concentrations through membranes made of HNPs with two different compositions, 100-17% and 500-35%. The results of these measurements are presented in Figure 6.

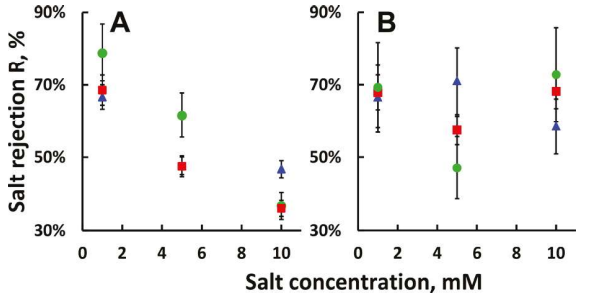

Figure 6. Salt rejection as a function of feed salt concentration (blue triangles: NaCl; green circles: $Na_3C_6H_5O_7$; red squares: Na_2SO_4): (A) 500-35% membrane; (B) 100-17% membrane.

The highest observed salt rejection was in the range of 70−80% for 1 mM salt solutions for both studied membranes, with salt rejection increasing with increasing co-ion charge as $R(\mathrm{NaCl}) < R(\mathrm{Na_2SO_4}) < R(\mathrm{Na_3C_6H_5O_7})$. Overall, rejection is surprisingly large, considering the relatively large pore size compared to pores of 1−22 nm reported previously for membranes with similar salt rejection.[67−69] In general, salt rejection is based on electrostatic repulsion, which depends on the pore charge and the Debye length of the electrolyte. For aqueous solutions of electrolytes at 25 °C, we calculate Debye lengths λ_D of ∼10 nm for 1 mM NaCl and λ_D of ∼1 nm for 10 mM citrate. As discussed above, pores in our HNP membranes have diameters of 30−100 nm and thus significantly exceed the Debye length, which would lead one to expect no substantial salt rejection. On the other hand, we previously demonstrated that the colloidal crystals of silica particles with relatively large charged nanopores are also capable of salt rejection.[26,37,38] For instance, in one experiment, we fabricated colloidal crystals composed of charged 440 nm silica spheres with pores of 68 nm diameter, as estimated based on a close-packed sphere model. Salt diffusion through these crystals was reduced by 50% at an electrolyte concentration of 0.05 M, corresponding to λ_D of ∼1.5 nm. Even if one assumes that electrolytes are repelled up to a distance of λ_D ∼5 nm away from the surface (∼7.5 nm, corresponding to the distance where the electro-

DOI: 10.1021/acsami.8b17483
ACS Appl. Mater. Interfaces 2019, 11, 3407−3416

static potential has decayed by 99%), a large cross-sectional area of the pore is still available for unhindered transport of charges. Thus, we speculated that the tortuous path through the colloidal crystal and its high surface area contribute to the observed electrostatic permselectivity. The HNP membranes studied here might deliver enhanced charge rejection for similar reasons.

Finally, we studied the salt rejection behavior of HNP membranes (Figure 6) as a function of solute concentration. We found that the membranes behaved differently depending on the polymer length and composition: Although the 100-17% HNP membranes showed similar charge rejection for all co-ions and all salt concentrations, the 500-35% HNP membranes displayed decreasing flux with increasing ion concentration.

Rejection of charged species by charged membranes as a function of salt concentration is often described using the Donnan model.[66] However, this model assumes that pores have a straight geometry, that charge rejection occurs solely because of the interactions between free salt ions and charges on the membrane surface, and it neglects the effects of steric hindrance.[54] Thus, the Donnan model can only provide a qualitative prediction of the behavior of HNP membranes. Specifically, salt rejection in HNP membranes is expected to increase with increasing co-ion charge, that is, $R(NaCl) < R(Na_2SO_4) < R(Na_3C_6H_5O_7)$, and with increasing number of sulfonic groups in the polymer chains due to increased charge density, and to decrease with increasing electrolyte concentration due to the screening of membrane charges by counterions.

The HNP membranes prepared using long brushes with the high number of charged groups (500-35%) follow this general trend. Salt rejection decreases with increasing salt concentration, and rejection of the trivalent co-ion is higher than that of di- and monovalent ions. The observed change in rejection of chloride and sulfate as a function of their concentration is similar to those reported for commercial nanofiltration membranes,[70] further supporting the notion that 500-35% HNP membranes behave as typical charged nanofiltration membranes.

On the other hand, the HNP membranes prepared using shorter polymer brushes with the lower number of charged groups (100-17%) showed a consistently high salt rejection (around 70%) regardless of co-ion valence or salt concentration. We hypothesize that, in this membrane, polymer swelling compensates for charge screening. Indeed, as discussed above, the short polymer brush undergoes significant swelling inside the nanopores (two times larger than the long polymer brush). This swelling should be accompanied by a significant increase in the number of charges inside the pore, which would compensate for the charge screening due to the higher electrolyte concentration.

Interestingly, citrate rejection in the presence of dextran improved significantly ($R_{citrate}$ ~81% as opposed to 62% for the pure salt solution of equal concentration) in 500-35% HNP membranes. This rejection enhancement can be explained in terms of a competition between specific (salt) and nonspecific (dextran) solutes to enter a pore: as the nonspecific solute enters a pore, available pore volume decreases, restricting the permeation of the salt through the nanopore.[21]

CONCLUSIONS

We have prepared novel nanoporous membranes by self-assembly of "hairy" SNPs carrying polyelectrolyte copolymer brushes. We showed that self-assembly can be controlled by polymer length and charge, which affect the interactions between the nanoparticles during membrane formation. We found, both experimentally and by modeling the interactions between the nanoparticles using MD simulations, that the properties of the membranes depend critically on the conformations of polymer chains inside the nanoconfined spaces of the nanoparticle assembly. The polymer plays three roles in the assembly and behavior of the membranes. First, it acts as a molecular glue, providing mechanical stability to the nanoparticle films. Second, the polymer chains extend to the interstitial spaces between the particles, thus defining the nanopore size. Finally, polymer chains introduce charged groups into the nanopores, which, combined with the high surface area and tortuosity of the nanopores, leads to high ion rejection by the nanopores despite their relatively large size. We also found that the polymer conformation responds to the ionic strength of the solution in interesting ways: long polymer brushes fill the nanopores and do not undergo significant swelling because of nanoconfinement, whereas short polymer brushes are able to swell two times more significantly. This leads to an unusual dependence of the salt rejection on salt concentrations because of the interplay of charge screening and polymer swelling.

Hairy nanoparticle membranes are easily prepared by assembly of accessible nanoscale building blocks, and their pore size is readily controlled in a broad range by changing the polymer length and silica core diameter. These membranes can be prepared with thicknesses ranging from a few micrometers to a few hundred micrometers and with a large surface area. Polyelectrolyte HNP membranes combine a number of favorable properties, including control of nanofiltration cutoff, control of permeability via responsive behavior, high charge rejection, high flux at low pressure, and tunable nanopore surface chemistry. Our findings suggest that HNP membrane may find applications in the areas of size- and charge-selective separations, water desalination, and in preparation of responsive membranes.

ASSOCIATED CONTENT

Supporting Information

The Supporting Information is available free of charge on the ACS Publications website at DOI: 10.1021/acsami.8b17483.

Side-view SEM images of the membranes (PDF)

AUTHOR INFORMATION

Corresponding Authors

*E-mail: michael.gruenwald@utah.edu (M.G.).
*E-mail: i.zharov@utah.edu (I.Z.).

ORCID

Michael Grünwald: 0000-0003-2186-1662
Ilya Zharov: 0000-0002-6292-8440

Author Contributions

†Yulia Eygeris and Emily V. White contributed equally to this work.

Notes

The authors declare no competing financial interest.

DOI: 10.1021/acsami.8b17483
ACS Appl. Mater. Interfaces 2019, 11, 3407−3416

■ ACKNOWLEDGMENTS

This work was supported by the National Science Foundation (grant no. CHE-1710052). The support and resources from the Center for High-Performance Computing at the University of Utah are gratefully acknowledged.

■ REFERENCES

(1) Scott, K. *Handbook of Industrial Membranes*, 1st ed.; Elsevier: Oxford, U.K., 1995.
(2) Mohammad, A. W.; Teow, Y. H.; Ang, W. L.; Chung, Y. T.; Oatley-Radcliffe, D. L.; Hilal, N. Nanofiltration Membranes Review: Recent Advances and Future Prospects. *Desalination* **2015**, *356*, 226−254.
(3) Pendergast, M. M.; Hoek, E. M. V. A Review of Water Treatment Membrane Nanotechnologies. *Energy Environ. Sci.* **2011**, *4*, 1946−1971.
(4) van Reis, R.; Zydney, A. Bioprocess Membrane Technology. *J. Membr. Sci.* **2007**, *297*, 16−50.
(5) Deng, J.; Toh, C.-S. Impedimetric DNA Biosensor Based on a Nanoporous Alumina Membrane for the Detection of the Specific Oligonucleotide Sequence of Dengue Virus. *Sensors* **2013**, *13*, 7774−7785.
(6) Adiga, S. P.; Jin, C.; Curtiss, L. A.; Monteiro-Riviere, N. A.; Narayan, R. J. Nanoporous Membranes for Medical and Biological Applications. *Wiley Interdiscip. Rev.: Nanomed. Nanobiotechnol.* **2009**, *1*, 568−581.
(7) Wei, L.; Kawamoto, K. Upgrading of Simulated Syngas by Using a Nanoporous Silica Membrane Reactor. *Chem. Eng. Technol.* **2013**, *36*, 650−656.
(8) *Membrane Technology: In the Chemical Industry*; Nunes, S. P.; Peinemann, K.-V., Eds.; Wiley-VCH: Weinheim, Germany, 2006, DOI: 10.1002/3527608788.
(9) Jons, S.; Ries, P.; McDonald, C. J. Porous Latex Composite Membranes: Fabrication and Properties. *J. Membr. Sci.* **1999**, *155*, 79−99.
(10) Siddique, H.; Peeva, L. G.; Stoikos, K.; Pasparakis, G.; Vamvakaki, M.; Livingston, A. G. Membranes for Organic Solvent Nanofiltration Based on Preassembled Nanoparticles. *Ind. Eng. Chem. Res.* **2013**, *52*, 1109−1121.
(11) Gin, D. L.; Noble, R. D. Designing the next Generation of Chemical Separation Membranes. *Science* **2011**, *332*, 674−676.
(12) van Rijn, P.; Tutus, M.; Kathrein, C.; Zhu, L.; Wessling, M.; Schwaneberg, U.; Böker, A. Challenges and Advances in the Field of Self-Assembled Membranes. *Chem. Soc. Rev.* **2013**, *42*, 6578−6592.
(13) Krieg, E.; Albeck, S.; Weissman, H.; Shimoni, E.; Rybtchinski, B. Separation, Immobilization, and Biocatalytic Utilization of Proteins by a Supramolecular Membrane. *PLoS One* **2013**, *8*, No. e63188.
(14) Pecinovsky, C. S.; Hatakeyama, E. S.; Gin, D. L. Polymerizable Photochromic Macrocyclic Metallomesogens: Design of Supramolecular Polymers with Responsive Nanopores. *Adv. Mater.* **2008**, *20*, 174−178.
(15) Averick, S.; Karácsony, O.; Mohin, J.; Yong, X.; Moellers, N. M.; Woodman, B. F.; Zhu, W.; Mehl, R. A.; Balazs, A. C.; Kowalewski, T.; et al. Cooperative, Reversible Self-Assembly of Covalently Pre-Linked Proteins into Giant Fibrous Structures. *Angew. Chem., Int. Ed.* **2014**, *53*, 8050−8055.
(16) Kaucher, M. S.; Peterca, M.; Dulcey, A. E.; Kim, A. J.; Vinogradov, S. A.; Hammer, D. A.; Heiney, P. A.; Percec, V. Selective Transport of Water Mediated by Porous Dendritic Dipeptides. *J. Am. Chem. Soc.* **2007**, *129*, 11698−11699.
(17) Wu, D.; Xu, F.; Sun, B.; Fu, R.; He, H.; Matyjaszewski, K. Design and Preparation of Porous Polymers. *Chem. Rev.* **2012**, *112*, 3959−4015.
(18) Deng, C.; Zhang, Q. G.; Han, G. L.; Gong, Y.; Zhu, A. M.; Liu, Q. L. Ultrathin Self-Assembled Anionic Polymer Membranes for Superfast Size-Selective Separation. *Nanoscale* **2013**, *5*, 11028−11034.
(19) Deng, J.; Liu, X.; Ma, L.; Cheng, C.; Shi, W.; Nie, C.; Zhao, C. Heparin-Mimicking Multilayer Coating on Polymeric Membrane via LbL Assembly of Cyclodextrin-Based Supramolecules. *ACS Appl. Mater. Interfaces* **2014**, *6*, 21603−21614.
(20) Kharlampieva, E.; Kozlovskaya, V.; Sukhishvili, S. A. Layer-by-Layer Hydrogen-Bonded Polymer Films: From Fundamentals to Applications. *Adv. Mater.* **2009**, *21*, 3053−3065.
(21) Sadeghi, I.; Kronenberg, J.; Asatekin, A. Selective Transport through Membranes with Charged Nanochannels Formed by Scalable Self-Assembly of Random Copolymer Micelles. *ACS Nano* **2018**, *12*, 95−108.
(22) Barry, E.; McBride, S. P.; Jaeger, H. M.; Lin, X.-M. Ion Transport Controlled by Nanoparticle-Functionalized Membranes. *Nat. Commun.* **2014**, *5*, 5847.
(23) Green, E.; Fullwood, E.; Selden, J.; Zharov, I. Functional Membranes via Nanoparticle Self-Assembly. *Chem. Commun.* **2015**, *51*, 7770−7780.
(24) Saeki, D.; Kawada, S.; Matsuyama, H. Preparation of Carboxylated Silver Nanoparticles via a Reverse Micelle Method and Covalent Stacking onto Porous Substrates via Amide Bond Formation. *Colloids Surf., A* **2018**, *552*, 98−102.
(25) Bohaty, A. K.; Smith, J. J.; Zharov, I. Free-Standing Silica Colloidal Nanoporous Membranes. *Langmuir* **2009**, *25*, 3096−3101.
(26) Smith, J. J.; Zharov, I. Ion Transport in Sulfonated Nanoporous Colloidal Films. *Langmuir* **2008**, *24*, 2650−2654.
(27) Gu, J.-E.; Lee, S.; Stafford, C. M.; Lee, J. S.; Choi, W.; Kim, B.-Y.; Baek, K.-Y.; Chan, E. P.; Chung, J. Y.; Bang, J.; et al. Molecular Layer-by-Layer Assembled Thin-Film Composite Membranes for Water Desalination. *Adv. Mater.* **2013**, *25*, 4778−4782.
(28) Escobar-Ferrand, L.; Li, D.; Lee, D.; Durning, C. J. All-Nanoparticle Layer-by-Layer Surface Modification of Micro- and Ultrafiltration Membranes. *Langmuir* **2014**, *30*, 5545−5556.
(29) Moffitt, M. G. Self-Assembly of Polymer Brush-Functionalized Inorganic Nanoparticles: From Hairy Balls to Smart Molecular Mimics. *J. Phys. Chem. Lett.* **2013**, *4*, 3654−3666.
(30) Fernandes, N. J.; Wallin, T. J.; Vaia, R. A.; Koerner, H.; Giannelis, E. P. Nanoscale Ionic Materials. *Chem. Mater.* **2014**, *26*, 84−96.
(31) Hui, C. M.; Pietrasik, J.; Schmitt, M.; Mahoney, C.; Choi, J.; Bockstaller, M. R.; Matyjaszewski, K. Surface-Initiated Polymerization as an Enabling Tool for Multifunctional (Nano-)Engineered Hybrid Materials. *Chem. Mater.* **2014**, *26*, 745−762.
(32) Akcora, P.; Liu, H.; Kumar, S. K.; Moll, J.; Li, Y.; Benicewicz, B. C.; Schadler, L. S.; Acehan, D.; Panagiotopoulos, A. Z.; Pryamitsyn, V.; et al. Anisotropic Self-Assembly of Spherical Polymer-Grafted Nanoparticles. *Nat. Mater.* **2009**, *8*, 354−359.
(33) Khabibullin, A.; Fullwood, E.; Kolbay, P.; Zharov, I. Reversible Assembly of Tunable Nanoporous Materials from "Hairy" Silica Nanoparticles. *ACS Appl. Mater. Interfaces* **2014**, *6*, 17306−17312.
(34) de Lannoy, C.-F.; Soyer, E.; Wiesner, M. R. Optimizing Carbon Nanotube-Reinforced Polysulfone Ultrafiltration Membranes through Carboxylic Acid Functionalization. *J. Membr. Sci.* **2013**, *447*, 395−402.
(35) Harrell, C. C.; Siwy, Z. S.; Martin, C. R. Conical Nanopore Membranes: Controlling the Nanopore Shape. *Small* **2006**, *2*, 194−198.
(36) Zharov, I.; Khabibullin, A. Surface-Modified Silica Colloidal Crystals: Nanoporous Films and Membranes with Controlled Ionic and Molecular Transport. *Acc. Chem. Res.* **2014**, *47*, 440−449.
(37) Newton, M. R.; Bohaty, A. K.; Zhang, Y.; White, H. S.; Zharov, I. pH- and Ionic Strength-Controlled Cation Permselectivity in Amine-Modified Nanoporous Opal Films. *Langmuir* **2006**, *22*, 4429−4432.
(38) Newton, M. R.; Bohaty, A. K.; White, H. S.; Zharov, I. Chemically Modified Opals as Thin Permselective Nanoporous Membranes. *J. Am. Chem. Soc.* **2005**, *127*, 7268−7269.
(39) Wang, T.; Long, Y.; Liu, L.; Wang, X.; Craig, V. S. J.; Zhang, G.; Liu, G. Cation-Specific Conformational Behavior of Polyelectrolyte Brushes: From Aqueous to Nonaqueous Solvent. *Langmuir* **2014**, *30*, 12850−12859.

DOI: 10.1021/acsami.8b17483
ACS Appl. Mater. Interfaces 2019, 11, 3407−3416

(40) Chu, X.; Yang, J.; Liu, G.; Zhao, J. Swelling Enhancement of Polyelectrolyte Brushes Induced by External Ions. *Soft Matter* **2014**, *10*, 5568−5578.
(41) Stöber, W.; Fink, A.; Bohn, E. Controlled Growth of Monodisperse Silica Spheres in the Micron Size Range. *J. Colloid Interface Sci.* **1968**, *26*, 62−69.
(42) McCarthy, P.; Tsarevsky, N. V.; Bombalski, L.; Matyjaszewski, K.; Pohl, C. Grafting Chromatographic Stationary Phase Substrates by Atom Transfer Radical Polymerization. *ACS Symp. Ser.* **2006**, *944*, 252−268.
(43) Khabibullin, A.; Minteer, S. D.; Zharov, I. The Effect of Sulfonic Acid Group Content in Pore-Filled Silica Colloidal Membranes on Their Proton Conductivity and Direct Methanol Fuel Cell Performance. *J. Mater. Chem. A* **2014**, *2*, 12761−12769.
(44) Dubois, M.; Gilles, K. A.; Hamilton, J. K.; Rebers, P. A.; Smith, F. Colorimetric Method for Determination of Sugars and Related Substances. *Anal. Chem.* **1956**, *28*, 350−356.
(45) Uttarwar, R. G.; Potoff, J.; Huang, Y. Study on Interfacial Interaction between Polymer and Nanoparticle in a Nanocoating Matrix: A Martini Coarse-Graining Method. *Ind. Eng. Chem. Res.* **2013**, *52*, 73−82.
(46) Marrink, S. J.; Risselada, H. J.; Yefimov, S.; Tieleman, D. P.; de Vries, A. H. The MARTINI Force Field: Coarse Grained Model for Biomolecular Simulations. *J. Phys. Chem. B* **2007**, *111*, 7812−7824.
(47) Anderson, J. A.; Lorenz, C. D.; Travesset, A. General Purpose Molecular Dynamics Simulations Fully Implemented on Graphics Processing Units. *J. Comput. Phys.* **2008**, *227*, 5342−5359.
(48) Glaser, J.; Nguyen, T. D.; Anderson, J. A.; Lui, P.; Spiga, F.; Millan, J. A.; Morse, D. C.; Glotzer, S. C. Strong Scaling of General-Purpose Molecular Dynamics Simulations on GPUs. *Comput. Phys. Commun.* **2015**, *192*, 97−107.
(49) Biesalski, M.; Johannsmann, D.; Rühe, J. Electrolyte-Induced Collapse of a Polyelectrolyte Brush. *J. Chem. Phys.* **2004**, *120*, 8807−8814.
(50) Choi, J.; Hui, C. M.; Schmitt, M.; Pietrasik, J.; Margel, S.; Matyjazsewski, K.; Bockstaller, M. R. Effect of Polymer-Graft Modification on the Order Formation in Particle Assembly Structures. *Langmuir* **2013**, *29*, 6452−6459.
(51) Daoud, M.; Cotton, J. P. Star Shaped Polymers : A Model for the Conformation and Its Concentration Dependence. *J. Phys.* **1982**, *43*, 531−538.
(52) Ohno, K.; Morinaga, T.; Takeno, S.; Tsujii, Y.; Fukuda, T. Suspensions of Silica Particles Grafted with Concentrated Polymer Brush: Effects of Graft Chain Length on Brush Layer Thickness and Colloidal Crystallization. *Macromolecules* **2007**, *40*, 9143−9150.
(53) Schaep, J.; Van der Bruggen, B.; Vandecasteele, C.; Wilms, D. Retention Mechanisms in Nanofiltration. In *Chemistry for the Protection of the Environment 3*; Pawłowski, L., Gonzales, M. A., Dudzińska, M. R., Lacy, W. J., Eds.; Springer: Boston, MA, 1998; pp 117−125, DOI: 10.1007/978-1-4757-9664-3_14.
(54) Wang, X.-L.; Tsuru, T.; Nakao, S.-I.; Kimura, S. The Electrostatic and Steric-Hindrance Model for the Transport of Charged Solutes through Nanofiltration Membranes. *J. Membr. Sci.* **1997**, *135*, 19−32.
(55) Applied Membranes Inc. Hollow fiber ultrafiltration membrane elements. https://www.appliedmembranes.com/hollow-fiber-ultrafiltration-membrane-elements-hf-uf-membranes.html (accessed Jul 14, 2018).
(56) Lanfrey, P.-Y.; Kuzeljevic, Z. V.; Dudukovic, M. P. Tortuosity Model for Fixed Beds Randomly Packed with Identical Particles. *Chem. Eng. Sci.* **2010**, *65*, 1891−1896.
(57) Carman, P. C. Fluid Flow through Granular Beds. *Chem. Eng. Res. Des.* **1997**, *75*, S32−S48.
(58) Khabibullin, A.; Zharov, I. Nanoporous Membranes with Tunable Pore Size by Pressing/Sintering Silica Colloidal Spheres. *ACS Appl. Mater. Interfaces* **2014**, *6*, 7712−7718.
(59) Zydney, A. L. High Performance Ultrafiltration Membranes: Pore Geometry and Charge Effects. *Membr. Sci. Technol.* **2011**, *14*, 333−352.
(60) Van der Bruggen, B.; Schaep, J.; Wilms, D.; Vandecasteele, C. Influence of Molecular Size, Polarity and Charge on the Retention of Organic Molecules by Nanofiltration. *J. Membr. Sci.* **1999**, *156*, 29−41.
(61) Granath, K. A.; Kvist, B. E. Molecular Weight Distribution Analysis by Gel Chromatography on Sephadex. *J. Chromatogr. A* **1967**, *28*, 69−81.
(62) Rogers, B. J.; Wirth, M. J. Slip Flow through Colloidal Crystals of Varying Particle Diameter. *ACS Nano* **2013**, *7*, 725−731.
(63) Yang, Z.; Tarabara, V. V.; Bruening, M. L. Adsorption of Anionic or Cationic Surfactants in Polyanionic Brushes and Its Effect on Brush Swelling and Fouling Resistance during Emulsion Filtration. *Langmuir* **2015**, *31*, 11790−11799.
(64) Schepelina, O.; Zharov, I. PNIPAAM-Modified Nanoporous Colloidal Films with Positive and Negative Temperature Gating. *Langmuir* **2007**, *23*, 12704−12709.
(65) Zhang, H.; Rühe, J. Swelling of Poly(methacrylic acid) Brushes: Influence of Monovalent Salts in the Environment. *Macromolecules* **2005**, *38*, 4855−4860.
(66) Schaep, J.; Van der Bruggen, B.; Vandecasteele, C.; Wilms, D. Influence of Ion Size and Charge in Nanofiltration. *Sep. Purif. Technol.* **1998**, *14*, 155−162.
(67) Van der Bruggen, B. Nanofiltration. In *Encyclopedia of Membrane Science and Technology*; Wiley: Hoboken, NJ, 2013; pp 1−22, DOI: 10.1002/9781118522318.emst077.
(68) Su, M.; Wang, D.-X.; Wang, X.-L.; Ando, M.; Shintani, T. Rejection of Ions by NF Membranes for Binary Electrolyte Solutions of NaCl, $NaNO_3$, $CaCl_2$ and $Ca(NO_3)_2$. *Desalination* **2006**, *191*, 303−308.
(69) Chan, E. P.; Mulhearn, W. D.; Huang, Y.-R.; Lee, J.-H.; Lee, D.; Stafford, C. M. Tailoring the Permselectivity of Water Desalination Membranes via Nanoparticle Assembly. *Langmuir* **2014**, *30*, 611−616.
(70) Peeters, J. M. M. Characterization of Nanofiltration Membranes. PhD Dissertation, Universiteit Twente, Enschede, Netherlands, 1997.

DOI: 10.1021/acsami.8b17483
ACS Appl. Mater. Interfaces 2019, 11, 3407−3416